arXiv:1402.3743v1 [cond-mat.quant-gas] 16 Feb 2014

Bright solitons in Bose-Einstein condensates with field-induced dipole moments

F Kh Abdullaev[1,2], A Gammal[3], B A Malomed[4] and Lauro Tomio[1,5]

[1]Instituto de Física Teórica, UNESP-Universidade Estadual Paulista, 01140-070, São Paulo, Brazil.
[2]Department of Physics, Kulliyyah of Science, International Islamic University of Malaysia, 25200, Kuantan, Malaysia.
[3]Instituto de Física, Universidade de São Paulo, 05508-090, São Paulo, Brazil.
[4]Department of Physical Electronics, School of Electrical Engineering, Faculty of Engineering, Tel Aviv University, Tel Aviv 69978, Israel.
[5]Centro de Ciências Naturais e Humanas (CCNH), Universidade Federal do ABC, 09210-170, Santo André, Brazil.

Abstract. We introduce an effectively one-dimensional (1D) model of a bosonic gas of particles carrying collinear dipole moments which are induced by an external polarizing field with the strength periodically modulated along the coordinate, which gives rise to an effective *nonlocal nonlinear lattice* in the condensate. The existence, shape and stability of bright solitons, appearing in this model, are investigated by means of the variational approximation and numerical methods. The mobility of solitons and interactions between them are studied too.

PACS numbers: 67.85.Hj, 03.75.Kk, 03.75.Lm

1. Introduction

Ultracold bosonic gases with dipole-dipole interactions (DDI) have drawn a great deal of attention in the last years, which is stimulated by new experimental achievements in the achievement of the Bose-Einstein condensation (BEC) in gases made of atoms carrying permanent magnetic moments, such as chromium [1], dysprosium [2], and erbium [3] , and the development of efficient theoretical methods for the analysis of such condensates [4]. The long-range and anisotropic character of the DDI leads to new physical phenomena, which are not expected in BEC with contact interactions, see reviews [5, 6, 7]. Among these phenomena well known are pattern-formation scenarios [8], the d-wave collapse [9], nonlocally coupled solitons in stacked systems [10], multidimensional anisotropic solitons [11], solitons in dipolar condensates in optical lattices [12, 13, 14, 15], and others. In addition to direct-current (dc) external magnetic fields, various configurations of dipolar condensates can be also controlled by combinations including alternating-current (ac) components [16, 17].

Another novel and potentially important ingredient available in BEC settings is spatially periodic modulation of the local strength of the contact interactions by means of the Feshbach resonance controlled by periodically patterned laser or magnetic fields, as considered, e.g., in [18], leading to the concept of optically or magnetically induced *nonlinear lattices*. The nonlinearity modulation in space gives rise to new types of solitons and solitary vortices, as summarized in review [19]. In particular, it was recently demonstrated that periodic modulation of the local orientation of permanent atomic or molecular dipole moments in an effectively one-dimensional (1D) setting, which may be induced by a periodically inhomogeneous external polarizing field, makes it possible to create DDI-induced *nonlocal* nonlinear lattices in atomic condensates [20]. The necessary periodic field structure can be built using the available technique of magnetic lattices [21], or similar ferroelectric lattices (see,e.g., Ref. [22]). The analysis in Ref. [20] was focused on 1D solitons in the dipolar condensate with periodic variations of the angle between dipoles.

Another possibility for the creation of nonlocal nonlinear lattices and the study of self-trapped matter-wave modes in them is to use a bosonic gas of polarizable particles, which do not carry permanent dipole moments, while a spatially periodic distribution of the dipolar density is *induced* by an external spatially varying *polarizing field* [17]. In particular, a promising possibility is to consider an ultracold gas of polarizable molecules, with dipole moments induced by a spatially modulated dc electric field (such periodic settings were not considered in [17]). The DDI in gases of field-induced dipoles may be very strong and give rise to a number of significant effects [6, 23, 17].

In the present work we consider a quasi-1D dipolar BEC with electric dipole moments of particles induced by the dc field with the local strength periodically varying in space, while its direction is uniform, being oriented along the system's axis, thus giving rise to the attractive DDI in the condensate (on the contrary to the repulsive interactions between induced dipoles polarized perpendicular to the system's axis or

plane, which was the subject of the analysis in [17]). The objective is to investigate the existence and stability of bright solitons in this system, controlled by the effective DDI-induced nonlocal nonlinear lattice. The mobility and collisions of the solitons are considered too.

The paper is organized as follows. The models is presented in Sec. II, which is followed by the study of the existence and stability of bright solitons in Sec. III. Results for dynamics and collision of solitons are reported in Sec. IV. Conclusions and perspectives are summarized in Sec. V.

2. The model

We consider the condensate elongated along axis x, with dipole moments of polarizable molecules or atoms induced by an external field directed along x too. The local strength of the polarizing field also varies along x. Accordingly, one can use the effectively one-dimensional (1D) Gross-Pitaevskii equation (GPE), with the DDI term derived from the underlying 3D GPE, as shown below. The necessary spatially modulated dc electric and/or magnetic field can be imposed, as said above, by ferroelectric or ferromagnetic lattices. Below, we consider local dipole moment induced by a polarizing electric field. One can also consider magnetic dipole moments induced by a solenoid, as shown at the end of this section.

In addition to the ferroelectric lattice, the periodic modulation of the strength of the electric field oriented *perpendicular* to the system's axis (x) can be provided by a capacitor with the separation between its electrodes modulated in x periodically, as per Eq. (23) written below, cf. Ref. [17]. However, the most essential part of the analysis is developed below for the periodically modulated strength of the electric field directed *along* x, to fix the attractive character of the respective DDI. This configuration of the electric field can be provided by a stacked capacitor built along the x axis (with the array of parallel electrodes made as grids, to prevent interference with the BEC flow along the axis), assuming periodic modulation of the dc voltage applied to adjacent pairs of electrodes.

The derivation of the 1D Gross-Pitaevskii equation

The GPE for the 3D mean-field wave function $\Psi(\mathbf{r},t)$ is

$$\begin{aligned} \mathrm{i}\hbar\frac{\partial\Psi}{\partial t} = & -\frac{\hbar^2}{2m}\nabla^2\Psi + \frac{m}{2}\left[\omega_\parallel^2 x^2 + d(x)\mathcal{E}(x) + \omega_\perp^2(y^2+z^2)\right]\Psi + \\ & + g_{3\mathrm{D}}|\Psi|^2\Psi + \left[\int |\Psi(\mathbf{r}',t)|^2 W_{\mathrm{DD}}(\mathbf{r}-\mathbf{r}')d^3\mathbf{r}'\right]\Psi, \end{aligned} \tag{1}$$

where $d(x)=\gamma\mathcal{E}(x)$ is the local dipole moment, induced by external field $\mathcal{E}(x)$, which is directed and modulated along x, γ is the molecular or atomic polarizability, $g_{3\mathrm{D}}$ is defined by the two-body scattering length a_s and atomic mass m: $g_{3\mathrm{D}}\equiv 4\pi\hbar^2 a_s/m$.

Further, the DDI kernel is given by

$$W_{\rm DD}(\mathbf{r}-\mathbf{r}') = \frac{d(x)d(x')}{|\mathbf{r}-\mathbf{r}'|^3}\left[1-\frac{3\,(x-x')^2}{|\mathbf{r}-\mathbf{r}'|^2}\right] \tag{2}$$

and the wave function is normalized to the number of atoms,

$$N = \int |\Psi(\mathbf{r},t)|^2\, d^3\mathbf{r}. \tag{3}$$

The field-induced dipole moment is essential in the range of

$$d\cdot\mathcal{E}\sim B, \tag{4}$$

where B is the rotational constant, determined by to the equilibrium internuclear distance r and reduced mass m_r of the polarizable molecule: $B=\hbar^2/(2m_r r^2)$ [6]. Typical values of the parameters are: $d\sim 1$ Debye, $B\sim h\times$ 10 GHz, which yields an estimate for the necessary electric-field strength, $\mathcal{E}\sim 10^4$ V·cm^{-1}. Such fields are accessible to experiments with BEC in atomic gases (see Appendix B of Ref. [6]).

Thus, the spatial variation of the strength of the polarizing dc electric field,

$$\mathcal{E}(x)=\mathcal{E}_0 f(x), \tag{5}$$

leads to the respective spatial modulation of the DDI, with $d(x)=d_0 f(x)$. In particular, the periodic variation of the field, such as that adopted below in Eq. (24), induces the above-mentioned effective nonlocal nonlinear lattice in the GPE.

To derive the equation for the wave function in the quasi-1D case, we use the method elaborated in Ref. [24]. If the ground state in the transverse plane, (y,z), is imposed by the trapping potential, the 3D wave function may be factorized as usual [25]

$$\Psi(\mathbf{r},t)=\psi(x,t)\left(\sqrt{\pi}a_\perp\right)^{-1}\exp\left(-\rho^2/2a_\perp^2\right), \tag{6}$$

with $\rho^2\equiv y^2+z^2$, and $a_\perp^2\equiv\hbar/m\omega_\perp$. Substituting this expression into (1) and integrating over (y,z), the effective one-dimensional DDI is derived with kernel

$$W_{\rm 1DD}=\frac{2d^2}{a_\perp^3}\left[\frac{2|x|}{a_\perp}-\sqrt{\pi}\left(1+\frac{2x^2}{a_\perp^2}\right)\exp\left(\frac{x^2}{a_\perp^2}\right)\mathrm{erfc}\left(\frac{|x|}{a_\perp}\right)\right], \tag{7}$$

where erfc is the complementary error function. Next, we introduce dimensionless variables,

$$x\to a_\perp x,\ \ t\to\frac{t}{\omega_\perp},\ \ \psi(x,t)\to\sqrt{\frac{5}{\pi^{3/2}a_d}}\phi(x,t),\ \ \alpha=\frac{\omega_\parallel^2}{2\omega_\perp^2},\ \ g=\frac{10a_s}{\pi^{3/2}a_d},$$

where $a_d=md^2/\hbar^2$ is the characteristic DDI length. Defining the rescaled polarizability, $\beta\equiv\gamma\mathcal{E}_0^2/2(a_\perp\omega_\perp)^2$, where $\mathcal{E}_0$ is the amplitude of modulated field (5), the original 3D GPE (1) is thus reduced to the 1D equation:

$$\mathrm{i}\frac{\partial\phi}{\partial t}=-\frac{1}{2}\frac{\partial^2\phi}{\partial x^2}+\alpha x^2\phi+\beta f^2(x)\phi+g|\phi|^2\phi-f(x)\phi\int_{-\infty}^{+\infty}f(x')|\phi'|^2R(x-x')dx', \tag{8}$$

where $\phi\equiv\phi(x,t)$ and $\phi'\equiv\phi(x',t)$, with the effective 1D kernel, following from Eq. (7) is (cf. Ref. [24]), given by

$$R(x)=\sigma\frac{10}{\pi}\left[\left(1+2x^2\right)\exp\left(x^2\right)\mathrm{erfc}(|x|)-\frac{2}{\sqrt{\pi}}|x|\right]. \tag{9}$$

Here we have added an extra parameter, which takes values $\sigma = +1$ for the attractive DDI, and $\sigma = -1/2$ for the repulsive DDI between dipoles oriented perpendicular to x, which makes it possible to consider the latter case too. Actually, the rather complex kernel (9) can be replaced by a simplified expression,

$$R(x) = \frac{10\sigma}{\pi\sqrt{\left(\pi\, x^2 + 1\right)^3}}, \tag{10}$$

which is very close to the exact one (9) [12], barring the fact that expression (10) is smooth near $x = 0$, while its counterpart (9) has a cusp at this point.

Note that the DDI can be represented by a pseudopotential which includes a contact-interaction (delta-functional) term [5, 26]. Then, spatially modulated $d(x)$ may induce a position-depending part of the contact interactions too. Such a combination of nonlinear local and dipolar lattices may be a subject of interest for a separate investigation. However, in the present setting, the regularization scale $a_\perp$ in kernel (7) eliminates the singular part of the DDI at scales $|x| \lesssim a_\perp$. Therefore, in the present work we restrict ourselves to the consideration of the pure nonlinear nonlocal lattice.

We assume that the dynamics of the system in the perpendicular directions is completely frozen, i.e., the transverse trapping frequency, $\omega_\perp$, is much larger then the longitudinal one, $\omega_\perp \gg \omega_{||}$. On the other hand, if $\omega_\perp$ is not too large, interesting transverse effects may occur, such as the Einstein-de Haas effect [27, 28, 29, 30], the consideration of which is beyond the scope of the present work.

In the potential given in Eq. (8) we can identify the usual harmonic-trap potential, αx^2, nonlinear term $g|\phi|^2\phi$ accounting for the collisional interaction, and an effective DDI potential, composed of linear and a nonlinear terms:

$$V_{\rm eff}^{\rm (DDI)}(x;|\phi|^2) = f(x)\left[\beta f(x) - \int_{-\infty}^{+\infty} f(x')|\phi'|^2 R(x-x')dx'\right], \tag{11}$$

where the modulation function [see Eq. (5)] is chosen, as said above, in the form of a periodic one:

$$f(x) = f_0 + f_1\cos(kx), \tag{12}$$

with the constant parameters f_0, f_1, and $k \equiv 2\pi a_\perp/\lambda = 2\pi/\Lambda$. Parameter β in Eq.(8) can vary from 1 to 10, under typical physical conditions, if the constant part of the modulation function is fixed as $f_0 \equiv 1$.

The Hamiltonian corresponding to Eq. (8) is

$$H = \int_{-\infty}^{+\infty} dx\left[\frac{1}{2}\left|\frac{\partial\phi}{\partial x}\right|^2 + \frac{g}{2}|\phi|^4 + \alpha x^2|\phi|^2 + \beta f^2(x)|\phi|^2\right] - \frac{1}{2}\int_{-\infty}^{+\infty} dx f(x)|\phi|^2\int_{-\infty}^{+\infty} dx' f(x')|\phi'|^2 R(x-x'). \tag{13}$$

Note that it contains not only the spatially modulated nonlinear DDI, but also the additional linear potential, $\beta f^2(x)$, which is induced by the interaction of the locally-induced dipole moment with the polarizing field, cf. Ref. [17]. The Hamiltonian term corresponding to this potential is denoted $H_{\rm DE}$ below.

Evaluation of parameters

The energy of the interaction of the dipole with the external electric field can be estimated, as per Eq. (4), as $H_{\rm DE} = d \cdot \mathcal{E} \sim B \sim h\times$ 10 GHz. As the total wave function is normalized to the number of atoms [see Eq. (3)], i.e., $|\Psi|^2 \sim N/a_\perp^3$, for the DDI energy we have

$$H_{\rm DD} = \int |\Psi|^2 W_{\rm DD}(r) d^3r \sim d^2 \frac{N}{a_\perp^3} \sim \frac{a_d \hbar^2}{m} \frac{N}{a_\perp^3}, \tag{14}$$

where the characteristic DDI length is $a_d = d^2 m/\hbar^2$. Therefore, with regard to $a_\perp^2 = \hbar/(m\omega_\perp)$, we obtain

$$H_{\rm DD} \sim N\,(a_d/a_\perp)\,\hbar\omega_\perp. \tag{15}$$

For $N \sim 10^5, \omega_\perp \sim 10^4$ Hz and $a_d \sim 10^4 a_s$, we thus conclude that $H_{\rm DE} \sim H_{\rm DD}$.

We note a peculiarity of the modulation period of the polarizing field in the dimensionless equation. Physical values of the period should be, evidently, on the order of or larger than the μm scale. The characteristic length related to $H_{\rm DE}$ is $l_d \sim \sqrt{\hbar^2/mB} \sim 10^{-2} a_\perp$. Further, we use an estimate $B \sim \hbar^2/(ml_d^2) = 10^4\hbar^2/(ma_\perp^2) = 10^4\hbar\omega_\perp$. Therefore, with $H_{\rm DE} \sim B$, we again obtain $H_{\rm DE} \sim H_{\rm DD}$. One possible way to suppress the interaction represented by $H_{\rm DE}$, and thus to focus on nonlinear DDI effects, is to decrease the induced dipolar moment d up to the level of 10^{-2} Debye (which remains experimentally observable [31]), and so to reduce $H_{\rm DE}$.

Another possible way is to suppress the linear-interaction term $H_{\rm DE}$, which was proposed in Ref. [17], is to consider the polarization imposed by a combination of dc and ac electric fields [32, 33, 34, 35, 36], oriented along the z- direction (i.e., perpendicular to the system's axis, x):

$$G(r) = F(r)[f_{\rm dc} + f_{\rm ac}\cos(\omega t)]\mathbf{e}_z, \tag{16}$$

Then the local dipolar moment $\mathbf{g} = g(t)\mathbf{e}_z$ of the atom or molecule is determined by the intrinsic equation of motion, considered here in the classical approximation [37]:

$$\frac{d^2g}{dt^2} + \omega_0^2 g + \Gamma\frac{dg}{dt} = F(r)[\lambda(0) f_{\rm dc} + \lambda(\omega) f_{\rm ac}\cos(\omega t)], \tag{17}$$

where ω_0 is the intrinsic eigenfrequency, Γ is the damping coefficient, while $\lambda(0) \equiv \lambda_0$ and $\lambda(\omega)$ are the effective static and dynamical susceptibilities, respectively. In the off-resonance situation, when the ac frequency, ω, is not too close to ω_0, the small dissipative term in Eq. (17) is negligible, which gives rise to the following solution:

$$g_{\rm off}(r) = F(r)\left[\frac{\lambda_0}{\omega_0^2} f_{\rm dc} + \frac{\lambda(\omega) f_{\rm ac}}{\omega^2 - \omega_0^2}\cos(\omega t)\right]. \tag{18}$$

On the other hand, close to the resonance the ac drive yields:

$$g_{\rm res}(r) = F(r)\frac{\lambda(\omega_0)}{\Gamma\omega_0}\sin(\omega_0 t). \tag{19}$$

These results lead to the following time-averaged DDI strength [17]:

$$\langle g_{\rm off}(r_1)g_{\rm off}(r_2)\rangle = F(r_1)F(r_2)\left[\frac{\lambda_0^2}{\omega_0^4}f^2{}_{\rm dc}+\frac{\lambda^2(\omega)f_{\rm ac}^2}{2(\omega_0^2-\omega^2)^2}\right], \tag{20}$$

$$\langle g_{\rm res}(r_1)g_{\rm res}(r_2)\rangle = F(r_1)F(r_2)\frac{\lambda^2}{2\Gamma^2\omega_0^2}.$$

In addition to the DDI, in the off-resonance situation the field-induced dipole moments give rise to the above-mentioned effective dipole-field interaction:

$$V_{\rm DE}(r) = -\langle g_{\rm off}G\rangle = -\left(F(r)\right)^2\left[\frac{\lambda_0}{\omega_0^2}f_{\rm dc}^2+\frac{\lambda(\omega)f_{\rm ac}^2}{2(\omega_0^2-\omega^2)}\right] = -\chi F^2(r), \tag{21}$$

where χ is the effective average polarizability, while in the resonant situation, with $f_{\rm dc}=0$, the substitution of expression (19) immediately yields $V_{\rm DE}(r)=0$. Then, it is obvious that potential (21) *vanishes* at $\omega=\Omega$, with Ω defined by equation

$$\frac{\Omega}{\omega_0} = \sqrt{1+\frac{\lambda(\Omega)}{2\lambda(0)}\frac{f_{\rm dc}^2}{f_{\rm ac}^2}}, \tag{22}$$

while the effective strength (20) does not vanish under condition (22):

$$\langle g_{\rm off}(r_1)g_{\rm off}(r_2)\rangle = F(r_1)F(r_2)\left[\frac{\lambda_0^2 f_{\rm dc}}{\omega_0^4}\left(1+2\frac{f_{\rm dc}^2}{f_{\rm ac}^2}\right)\right].$$

In the case when the local dipole moment is induced by magnetic field, we consider the field with a fixed (x) orientation, produced by a solenoid of diameter D, periodically varying along the solenoid's axis, $D=D(x)$, with period L, such as

$$D(x) = D_0 + D_1\cos\left(2\pi x/L\right). \tag{23}$$

The local magnetic field in this configuration is

$$\mathcal{H} = \frac{\Phi}{\pi D^2(x)} = \Phi\left[D_0+D_1\cos\left(\frac{2\pi x}{L}\right)\right]^{-2} \approx \frac{\Phi}{\pi D_0^2}\left[1-2\frac{D_1}{D_0}\cos\left(\frac{2\pi x}{L}\right)\right], \tag{24}$$

where Φ is the magnetic flux trapped in the solenoid, and the approximation is valid for $D_1/D_0 \ll 1$. It should be noted that this scheme requires a strong magnetic field, which can be difficult to achieve in the experiments. Therefore, in this work we actually consider induced electric dipole moments.

3. Bright solitons: existence and stability

The existence of bright-soliton solutions can be investigated by solving the corresponding eigenvalue problem, obtained from Eqs. (8) and (11), with $\phi = |\phi|e^{-{\rm i}\mu t}$:

$$-\frac{1}{2}\frac{\partial^2\phi}{\partial x^2}+\alpha x^2\phi+g|\phi|^2\phi+V_{eff}^{DDI}(x;|\phi|^2)\phi = \mu\phi. \tag{25}$$

We consider full numerical solutions of Eq. (25), as well as corresponding variational approaches (VA), for two characteristic cases, as defined in the next sub-sections. The VA results will be compared with the numerical solutions.

3.1. The variational approximation for $\alpha = 0$, $\beta \neq 0$.

To derive the VA, we start from the averaged Lagrangian, $L = \int_{-\infty}^{+\infty} \mathcal{L} dx$, with density

$$\mathcal{L} = \mu|\phi|^2 - \frac{1}{2}\left|\frac{d\phi}{dx}\right|^2 - \beta\left[f(x)\right]^2|\phi|^2 - \frac{g}{2}|\phi|^4 + \frac{f(x)}{2}|\phi|^2\int_{-\infty}^{+\infty} f(x')R(x-x')|\phi'|^2 dx'. \quad (26)$$

For the wave function of the condensate, we assume the following Gaussian ansatz with center set at $x = \zeta$:

$$\phi = A\exp\left(-\frac{(x-\zeta)^2}{2a^2}\right). \quad (27)$$

The corresponding averaged Lagrangian L is given by

$$\frac{L}{N} = \mu_r - \frac{1}{4a^2} - \beta\left(2f_1 f_0 e^{-a^2k^2/4}\cos(k\zeta) + \frac{f_1^2}{2}e^{-a^2k^2}\cos(2k\zeta)\right) - \frac{gN}{2\sqrt{2\pi}a} + \frac{N}{2\pi a^2}F(a,\zeta,f_0,f_1),$$

where we have $N = \sqrt{\pi}A^2 a$, $\mu_r \equiv \mu - \beta\left[f_0^2 + (1/2)f_1^2\right]$, and

$$F(a,\zeta,f_0,f_1) \equiv \int_{-\infty}^{+\infty} dx f(x) e^{-[(x-\zeta)/a]^2}\int_{-\infty}^{+\infty} dy f(y)R(x-y)e^{-[(y-\zeta)/a]^2}. \quad (28)$$

By means of a variable transformation, with R defined by Eq. (10), F can be represented in terms of single-variable integrals:

$$F(a,\zeta,f_0,f_1) = \left[f_0^2 + \frac{1}{2}f_1^2\cos\ (2k\zeta)e^{-(ka)^2/2}\right]h_0(a) + \frac{1}{2}f_1^2 h_2(a) + 2f_0 f_1\cos(k\zeta)e^{-(ka)^2/8}h_1(a), \quad (29)$$

where

$$h_n(a)|_{n=0,1,2} \equiv \frac{10\sigma}{\sqrt{\pi}}a\int_{-\infty}^{+\infty} dz\frac{e^{-(z/a)^2}}{\sqrt{2\pi\ z^2+1}^3}\cos\left(\frac{nkz}{\sqrt{2}}\right). \quad (30)$$

The corresponding Euler-Lagrange equations, $\partial L/\partial N = \partial\ L/\partial a = \partial L/\partial\zeta = 0$, take the following form:

$$\mu\ = \frac{1}{4a^2} + \left(\sqrt{2\pi}ga - 2F\right)\frac{N}{2\pi a^2} + \beta\left[f_0^2 + \frac{f_1^2}{2}\left(1 + e^{-(ka)^2}\cos(2k\zeta)\right) + 2f_0 f_1 e^{-(ka/2)^2}\cos(k\zeta)\right], \quad (31)$$

$$N = 2\pi\frac{1 + 2\beta(ka^2)^2 f_1\left[f_0 e^{-(ka/2)^2}\cos(k\zeta) + f_1 e^{-(ka)^2}\cos(2k\zeta)\right]}{4F - 2a\partial F/\partial a - \sqrt{2\pi}ga}, \quad (32)$$

$$\zeta\ = 0,\ \ \pi/k,\ \ 2\pi/k, ..., \quad (33)$$

where $F \equiv F(a,\zeta,f_0,f_1)$. The condition (33) leads to two solutions ($\cos(k\zeta) = \pm 1$), which correspond to changing the relative signs of the constants f_0 and f_1, and Eqs.

(31) and (32) can be written as

$$\mu_{\pm} = \frac{1}{4a^2} + \beta\left[f_0^2 + \frac{1}{2}f_1^2(1+e^{-(ka)^2}) \pm 2f_0 f_1 e^{-(ka/2)^2}\right] + \left(\sqrt{2\pi}ga - 2F_{\pm}\right)\frac{N_{\pm}}{2\pi a^2}, \tag{34}$$

$$N_{\pm} = 2\pi\frac{1+2\beta(ka^2)^2 f_1(f_1 e^{-(ka)^2} \pm f_0 e^{-(ka/2)^2})}{4F_{\pm} - 2a\partial F_{\pm}/\partial a - \sqrt{2\pi}ga}, \tag{35}$$

where $F_+ \equiv F(a, 0, f_0, f_1)$ and $F_- \equiv F(a, \pi/k, f_0, f_1)$.

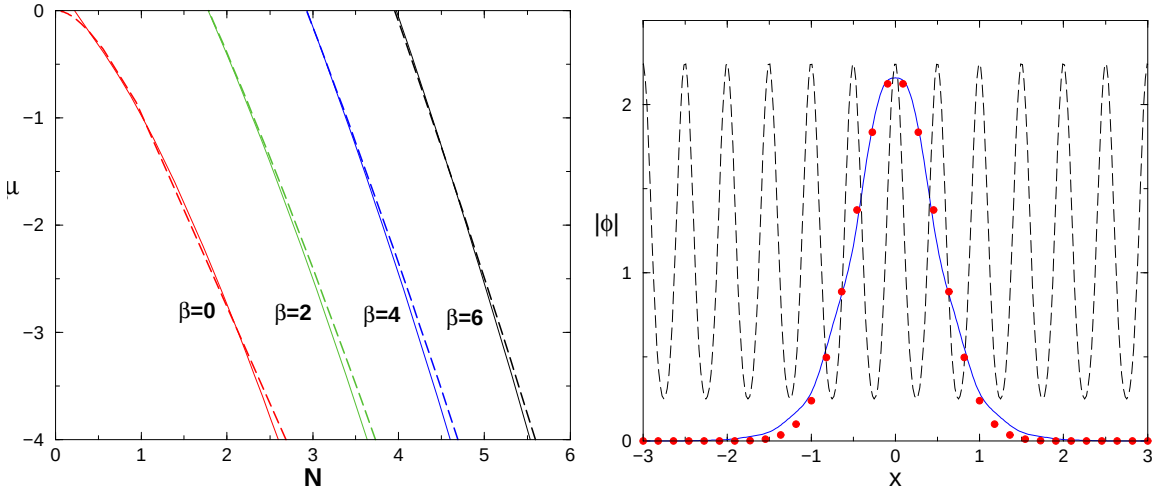

Figure 1. Left panel: chemical potential μ as a function of norm N, obtained from direct numerical solutions of Eq. (25) (solid lines), and from the corresponding variational approach (dashed lines). This figure stresses the effect of the nonlinearity parameter, β (the scaled polarizability) on the results. Other parameters are $\alpha = g = 0$, $\sigma = 1$, $f_0 = 1$, $f_1 = 0.5$ and $\Lambda = 0.5$ (corresponding to $k = 4\pi$). Right panel: the numerical solution (the solid line) for the profile of the wave function, centered in $x = 0$, is compared to the corresponding variational result (the dotted curve), for $\beta = 6$ and $\mu = 0$. In this right panel, we also plot function $f^2(x)$ by dashed line.

The solutions produced by the VA are compared with their numerically found counterparts in Figs. 1 and 2, for $g = \alpha = 0$, $f_0 = 1$, $f_1 = 0.5$, and $\Lambda = 0.5$ ($k = 4\pi$). The corresponding numerical solutions of Eq. (25) were obtained by means of the relaxation technique, as described in Ref. [38]. The effect of parameter β is illustrated by plots of chemical potential μ versus the number of atoms, N, in the left panel of Fig. 1. The figure demonstrates that the VA provides good agreement with the numerical results. Variational and numerically found profiles of the solitons are compared in the right panel of the figures, for $\mu = 0$ and $\beta = 6$. In the right panel, we also show the oscillatory function, $f^2(x)$, by the dashed line.

The variational approach produces more accurate results for large β because, in this case, the contribution of the linear lattice grows, and it is known that the Gaussian ansatz, that we use here, works well with linear lattice potentials [19]. Further, the

steady increase of μ with β in the left panel of Fig. 1 is also explained by the fact that the linear potential in Eq. (8) is multiplied by β.

In the top panel of Fig. 2, for $k = 2$ ($\Lambda = \pi$) and $\beta = 6$, with the other parameters the same as in Fig. 1, the numerical results for the $\mu(N)$ dependences are shown in three distinct regions: two stable (1 and 3) and one unstable (region 2). The profiles, displayed in the left bottom panel, clearly show that the wave function profiles are centered at $x = \pi/2$ in stable region 1. In unstable region 2, we verify a transition from stable region 1 to stable region 3, with the center of the profiles moving to $x = 0$. For the reference's sake, the effective DDI potential, as defined by Eq. (11), is displayed in the right bottom panel for three values of the chemical potential. A noteworthy feature is asymmetry with respect to the reflection, $x \to -x$, which can also be observed in the profiles shown in the left bottom panel of Fig. 2.

As seen in Fig. 2, the VA gives a perfect agreement with the numerical solutions in region 1 (where the center of the profile is located at $x = \zeta = \pi/2$), when $\mu > -2$, and in region 3 (where the center of the profile is at $x = \zeta = 0$), when $\mu < -9$. However, the VA cannot follow the behavior presented by the numerical results in region 2, because the simple Gaussian ansatz is not an adequate one, in this case. In the top panel, we also present the corresponding total energy, obtained from the numerical solutions. In the left bottom panel, together with the profiles, $f^2(x)$ is displayed by the dashed line.

For the perpendicular orientation of the dipoles, corresponding to the repulsive DDI, $\sigma = -1/2$ (while other parameters are the same as in 2), we demonstrate in Fig. 3, by means of numerical results for different values of μ, that the wave-function profiles are delocalized, i.e., they do not build bright solitons.

In Fig. 4, we present numerical results for $\mu(N)$ (the left panels), compared with VA findings for $\beta = 0$, in the absence of the linear trap ($\alpha = 0$). In the left panels we consider different values of f_1, with $\Lambda = 1$ (left top) and 0.5 (left bottom). According to the Vakhitov-Kolokolov (VK) criterion, the solutions may be stable if the condition $\partial\mu/\partial N < 0$ holds [39]. This assumption is well verified by our numerical results, for the whole range of parameters that we have analyzed. Simulations of the corresponding temporal evolution (not shown in this figure) validate the VK criterion in the present model. However, the VA results cannot follow the results to the full extension, besides the fact that they present very good agreement for large negative values of μ. As seen in the left top panel of Fig. 4 , for $\Lambda = 1$ the VA correctly predicts the stability and converges to numerical results for $\mu < -1.5$ at all values of f_1. In the case of $\Lambda = 0.5$ (the left bottom panel), the VA results are equally accurate at $\mu < -6$. On the other hand, in the case of $f_1 = 2.0$ and $\Lambda = 0.5$, the VA results represent a set of two solutions, one being nearly insensitive to variations of f_1.

3.2. The pure nonlocal nonlinear lattice ($\alpha = \beta = 0$)

Fixing $\alpha = 0$ and $\beta = 0$, we have analyzed the model with the repulsive contact interactions ($g > 0$). The corresponding term in Eq. (1) tends to expand the wave

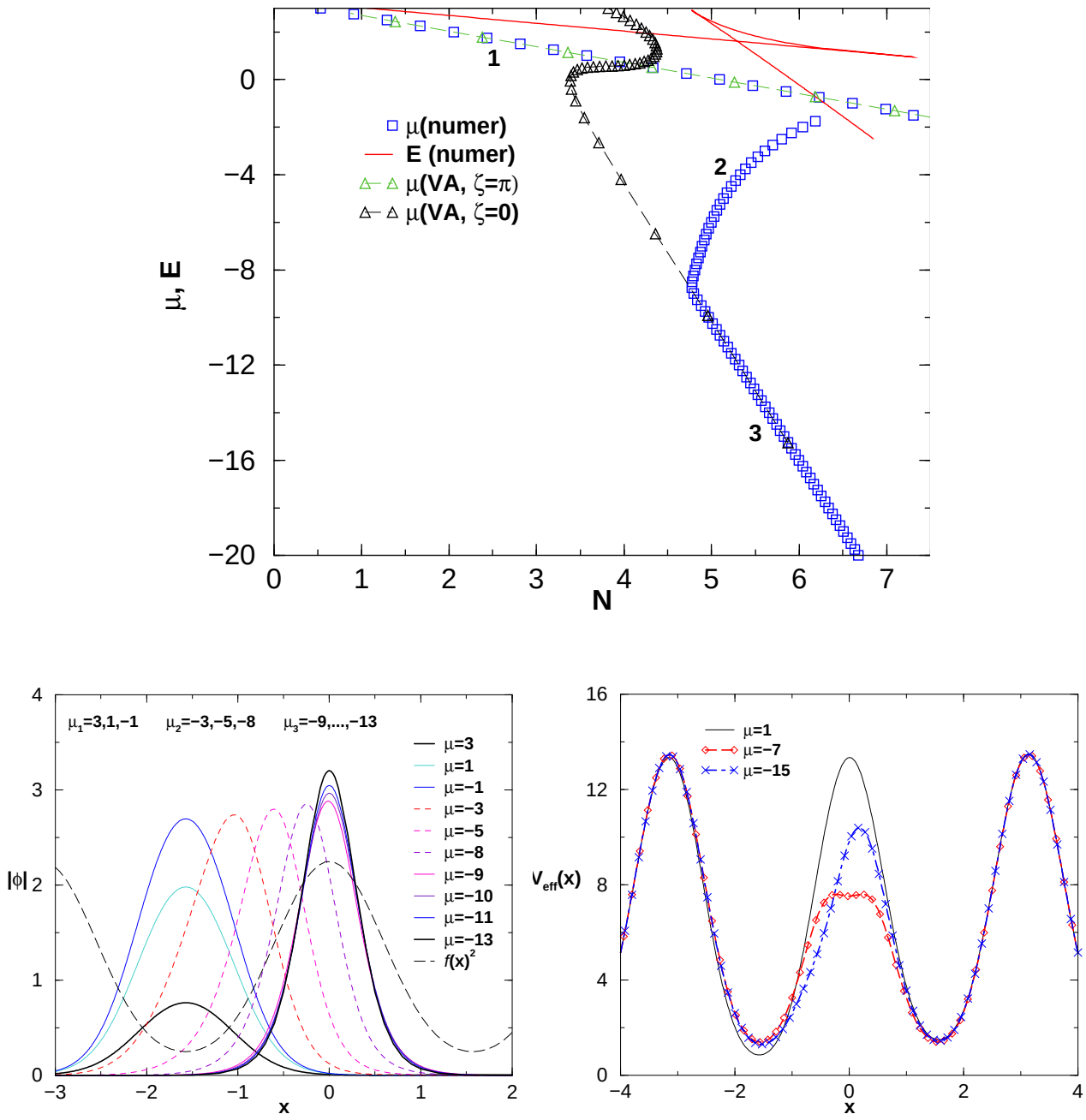

Figure 2. The top panel: chemical potentials, as obtained from numerical solutions and from the VA, are shown for $\Lambda = \pi$ (i.e., $k = 2$). Other parameters are $\alpha = g = 0$, $\sigma = 1$, $f_0 = 1$, $f_1 = 0.5$ and $\beta = 6$. In this panel, we indicate three regions (1, 2 and 3) for the numerical solutions, following the variation of the chemical potential (μ_1, μ_2 and μ_3), to identify the corresponding profiles that are shown in the left-bottom panel. For the reference, in the top panel we also plot the total energy (solid-red line), as obtained from the numerical solution. The modulation function, $f^2(x)$, is shown by the black-dashed line in the left bottom panel. The numerical results for the corresponding effective DDI potential, given in Eq.(11), are shown in the right-bottom panel for three different values of the chemical potential.

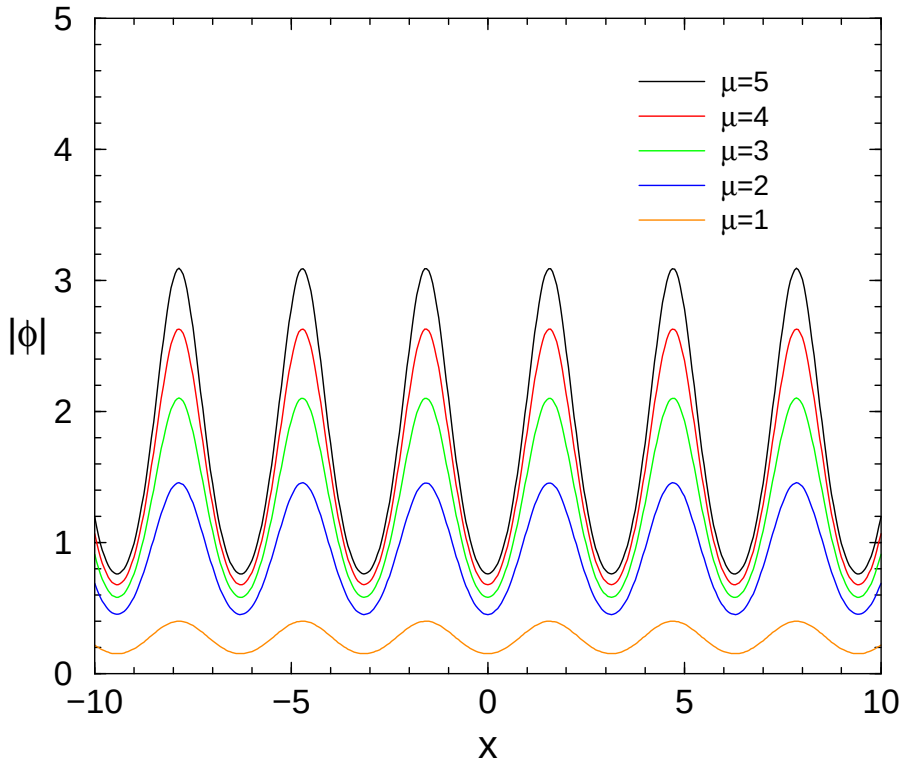

Figure 3. (Color online) Solution profiles for $\sigma = -1/2$, with other parameters the same as in Fig. 2 (in particular, $\Lambda = \pi$ and $\beta = 6$).

function, on the contrary to the attractive nonlocal nonlinear interaction, cf. Ref. [12]. In Fig. 5, fixing other parameters as $f_0 = 1$, $f_1 = 0.5$, $\Lambda = 0.5$, and $\mu = -2$, we present stationary solutions for different magnitudes of g, in the left panel. As g increases, the wave function indeed gets broader and the number of atoms trapped in the soliton increases. Beyond a critical value, $g_c = 3.45$, no solution can be found. In the right panel of Fig. 5, keeping the chemical potential μ and the other parameters, given in the left panel, fixed, we present g_c and the corresponding value of N for different values of f_1. It is observed that N decreases and g_c increases with the increase of f_1.

This dependence can be explained considering the broad soliton case. Then the nonlocal term can be approximated as the local one with an effective nonlinearity coefficient,

$$\gamma_{\text{eff}} = f^2(x) \int_{-\infty}^{+\infty} dy R(y)$$

and the bright solitons should exist, provided that $g > f^2 \int_{-\infty}^{+\infty} dy R(y)$. This arguments explain the growth of g_c with the increase of f_1, as observed in the right panel of Fig. 5.

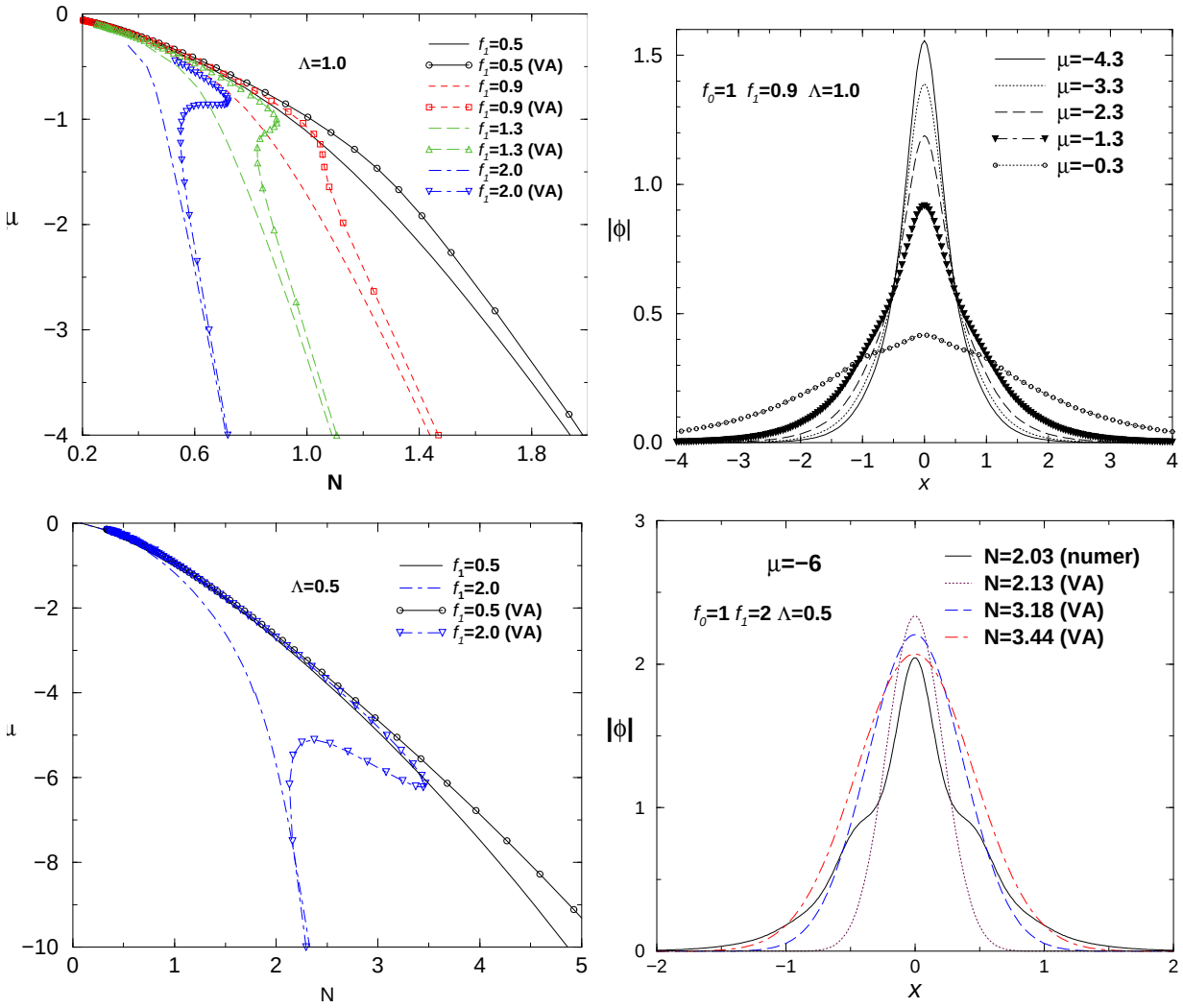

Figure 4. (Color online) Left panels: plots $\mu(N)$, for different values of f_1 (as indicated in the frames), with $\beta = 0$, $f_0 = 1$, and $\Lambda = 1$ or 0.5 (the top and bottom panels, respectively). In the right top frame, numerically found profiles are displayed for different values of μ, corresponding to the case with $f_1 = 0.9$, which is shown in the left-top panel. In the right-bottom frame, we consider the case with $\mu = -6$ and $f_1 = 2$, where three variational profiles are displayed for different values of N.

4. Dynamics of bright solitons

In this section we address the mobility of solitons and their collisions. The soliton motion in nonlinear lattices was previously considered in Refs. [40, 41, 42, 43]. First, we present full numerical solutions of the 1D GPE (8), exploring a parameter region for finding stable bright-solitons solutions. This is followed by consideration of a dynamical version of the variational approach, with some results for frequencies of oscillations of perturbed solitons being compared with the full numerical calculations.

The propagation of a soliton is presented in two panels of Fig. 6. In the left panel, for $\mu = -1$ and $N \approx 1.02$, we show the soliton propagation by considering, in the

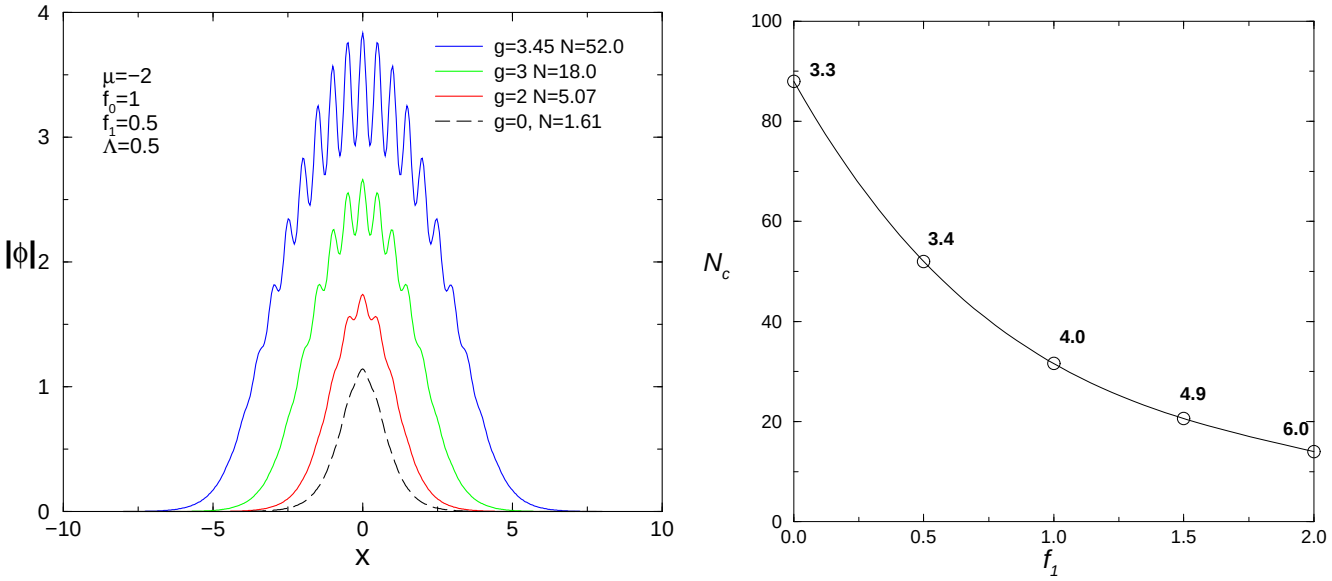

Figure 5. (Color online) The left panel: numerical results for the wave-function profiles with fixed $\mu = -2$ and a few values of the contact-interaction strength g. The corresponding values of N are indicated inside the panel. Other parameters are $f_0 = 1$, $f_1 = 0.5$ and $\Lambda = 0.5$. These results for $f_1 = 0.5$ define critical maximum values $g_c = 3.45$ and $N_c = 52$, above which no bright soliton were found. In the right panel, varying modulation amplitude f_1 in the interval of $0 \leq f_1 \leq 2$ and keeping other parameters as in the left panel, we display a curve corresponding to the critical values of N and g. Critical values g_c are indicated for some data points along the curve.

dimensionless units, a time interval from 0 to 20, and velocity equal to 1. In the right panel, we present the case of $\mu = -10$ and $N \approx 4.86$, showing profiles separated by time intervals $\Delta t = 2$. In the latter case, the soliton ends up getting trapped at a fixed position. In both the cases, we have $\alpha = \beta = g = 0$, and $f_0 = 1$, $f_1 = 0.5$, $\Lambda = 0.5$.

The interaction of two solitons is shown in four panels of Fig. 7, for $\mu = -10$ and $N \approx 4.86$. The field profiles are displayed with time intervals $\Delta t = 0.1$, the average velocity being zero. The parameters are the same as in Fig. 6 ($f_0 = 1$, $f_1 = 0.5$ and $\Lambda = 0.5$). We consider the solitons with zero phase difference between them, hence they attract each other. These panels display a transition from a bound state to a breather. The density plot corresponding to the results presented in Fig. 7 is displayed in Fig. 8. For the same parameters, we have verified that the solitons demonstrate almost no interaction when the phase shift between them is π.

Next, for the comparison with numerical solutions, we here present a dynamical version of the VA, which is based on the following Gaussian ansatz:

$$\phi(x,t) = A(t) \exp\left\{ -\frac{[x-\zeta(t)]^2}{2\,(a(t))^2} + \mathrm{i}b(t)\,[x-\zeta(t)]^2 + \mathrm{i}\kappa(t)\,[x-\zeta(t)] - \mathrm{i}\mu t \right\}. \quad (36)$$

To derive evolution equations for soliton parameters A, a, ζ, b, k, p, we calculate the

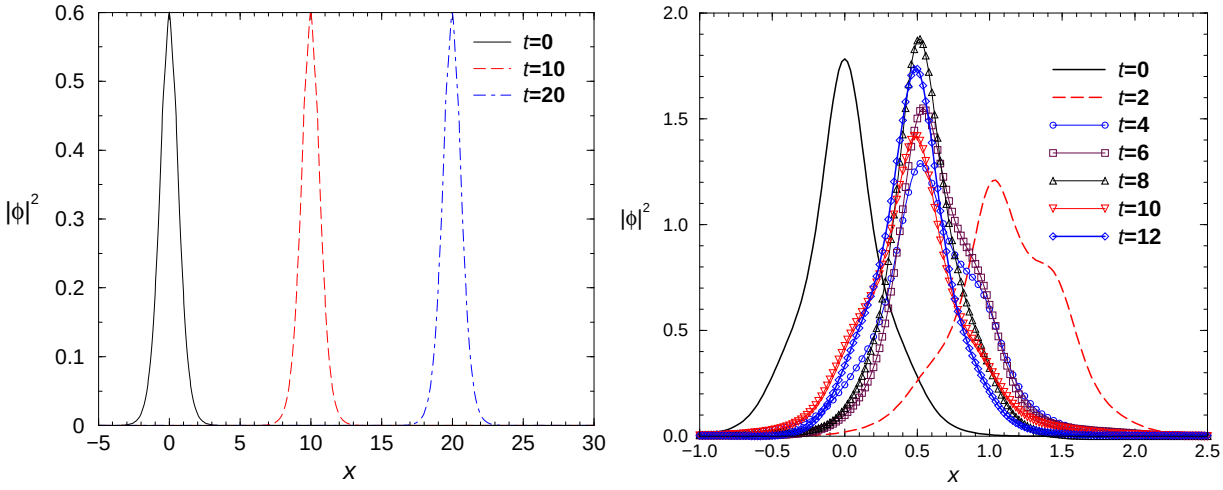

Figure 6. (Color online) Propagation of a soliton. In the left panel, soliton profiles are shown with time intervals $\Delta t = 10$ (the velocity is 1), for $\mu = -1$ and $N \approx 1.02$. In the right panel, $\mu = -10$, $N \approx 4.86$, with the profiles shown with intervals $\Delta t = 2$. In both cases, $f_0 = 1$, $f_1 = 0.5$ and $\Lambda = 0.5$ (with $\alpha = \beta = 0$).

respective averaged Lagrangian, taken with the full dynamical density

$$\mathcal{L}(x,t) = \mathrm{Im}\left(\phi\frac{\partial\phi^*}{\partial t}\right) - \frac{1}{2}\left|\frac{\partial\phi}{\partial x}\right|^2 - (\alpha x^2 + \beta f(x)^2)|\phi|^2 - \frac{g}{2}|\phi|^4 + \frac{f(x)|\phi|^2}{2}\int_{-\infty}^{\infty} dx' R(x-x')f(x')|\phi(x')|^2,$$

cf. its static counterpart (26). The averaged Lagrangian per particle is given by

$$\frac{L}{N} = -\frac{1}{2}a^2\frac{db}{dt} + \kappa(t)\frac{d\zeta}{dt} + \mu_r - \frac{1}{4a^2} - a^2b^2 - \frac{1}{2}\kappa(t)^2 - \frac{\alpha}{2}a^2 - \alpha\zeta^2 - 2\beta f_0 f_1\cos(k\zeta)e^{-a^2k^2/4} - \frac{\beta}{2}f_1^2\cos(2k\zeta)e^{-a^2k^2} - \frac{gN}{2\sqrt{2\pi}a} + \frac{NF}{2\pi a^2}, \quad (37)$$

where, as in the static setting, we have $N = \sqrt{\pi}A^2a$, with $F \equiv F(a,\zeta,f_0,f_1)$ given by Eq. (28). The Euler-Lagrange equations following from Lagrangian (37) give rise to the coupled evolution equations for the soliton's width and location of the center of mass:

$$a_{tt} \equiv \frac{d^2a}{dt^2} = \frac{1}{a^3} - 2\alpha a + 2ak^2\beta f_1\left[f_0\cos(k\zeta)e^{-a^2k^2/4} + f_1\cos(2k\zeta)e^{-a^2k^2}\right] + \frac{gN}{\sqrt{2\pi}a^2} - \frac{2NF}{\pi a^3} + \frac{N}{\pi a^2}\frac{\partial F}{\partial a} = -\frac{\partial U_a}{\partial a}, \quad (38)$$

$$\zeta_{tt} \equiv \frac{d^2\zeta}{dt^2} = -2\alpha\zeta + 2k\beta f_1\sin(k\zeta)\left[f_0e^{-a^2k^2/4} + f_1\cos(k\zeta)e^{-a^2k^2}\right] + \frac{N}{2\pi a^2}\frac{\partial F}{\partial\zeta} = -\frac{\partial U_\zeta}{\partial\zeta}, \quad (39)$$

from where the following effective potentials are identified:

$$U_a = \alpha a^2 + \frac{1}{2a^2} + 4\beta f_0 f_1\cos(k\zeta)e^{-a^2k^2/4} + \beta f_1^2\cos(2k\zeta)e^{-a^2k^2} + \frac{gN}{\sqrt{2\pi}a} - \frac{NF}{\pi a^2}, \quad (40)$$

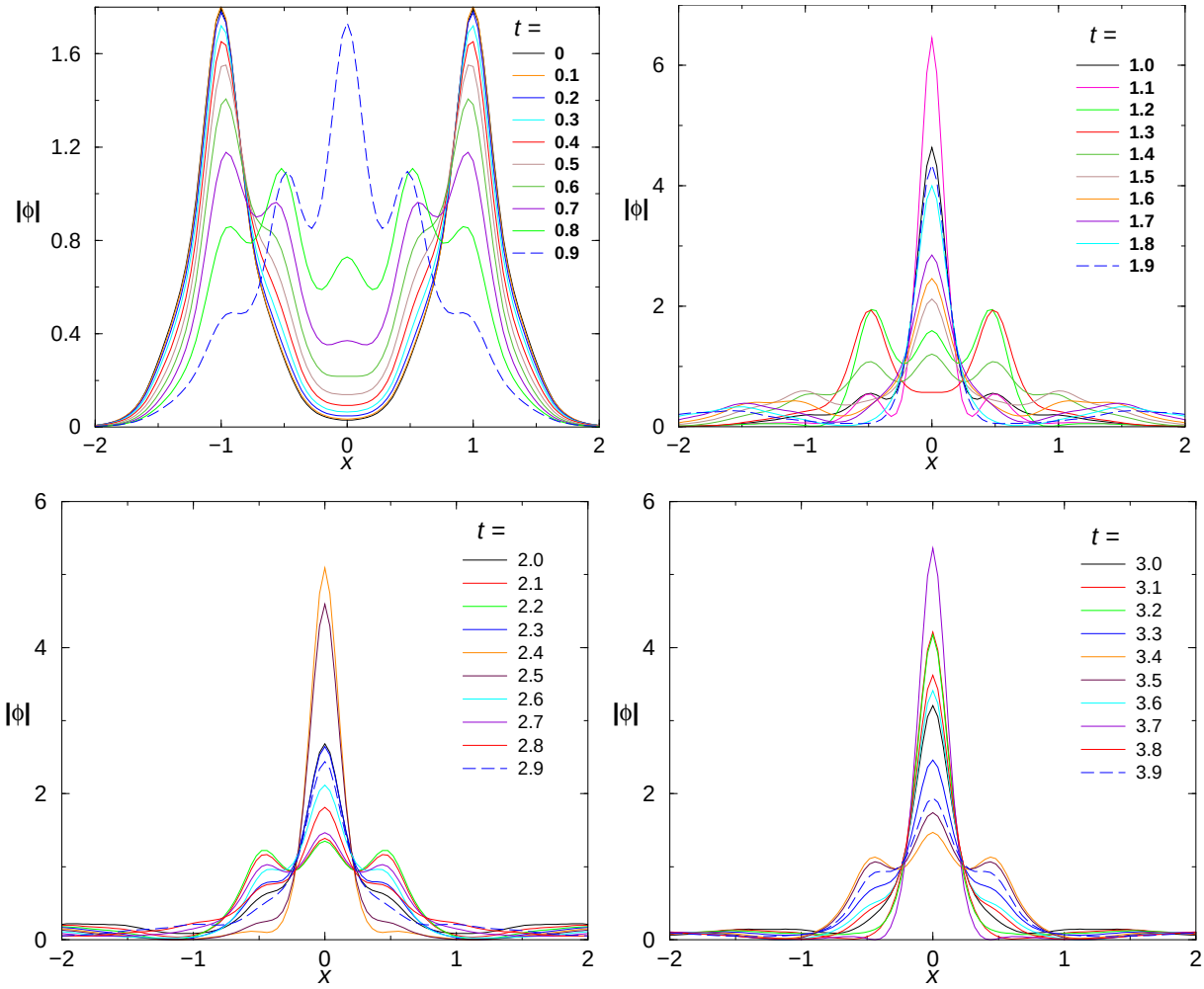

Figure 7. (Color online) The interaction of two solitons, with $\mu = -10$, $N \approx 4.86$, is shown in four panels at different moments of time, with $\Delta t = 0.1$ (the average velocity is zero), as indicated in the panels. In all the cases, parameters are $f_0 = 1$, $f_1 = 0.5$ and $\Lambda = 0.5$ ($a_\perp = 2, \lambda = 1$). The phase difference between the solitons is zero, therefore they attract each other. One can see a transition from a bound state to a breather.

$$U_\zeta = \alpha\zeta^2 + 2\beta f_0 f_1 \cos(k\zeta) e^{-a^2k^2/4} + \frac{\beta}{2} f_1^2 \cos(2k\zeta) e^{-a^2k^2} - \frac{NF}{2\pi a^2}. \tag{41}$$

Frequencies of small oscillations for the width and center of mass can be obtained from Eqs. (38-41). To this end, we set $\zeta = \zeta_s + \delta\zeta, \delta\zeta \ll \zeta_s$, where ζ_s is the fixed point, and $a = a_s + \delta a, \delta a \ll a$. By linearizing Eq. (38) in δ_a, and Eq. (39) in δ_ζ, respectively, we find

$$\delta a_{tt} = \frac{\partial a_{tt}}{\partial a}\delta a + \frac{\partial a_{tt}}{\partial \zeta}\delta\zeta, \tag{42}$$

$$\delta\zeta_{tt} = \frac{\partial \zeta_{tt}}{\partial \zeta}\delta\zeta + \frac{\partial \zeta_{tt}}{\partial a}\delta a, \tag{43}$$

from where we can derive the corresponding frequencies:

$$\omega_a^2 = -\frac{\partial a_{tt}}{\partial a} = 2\alpha + \frac{3}{a_s^4} + \beta k^2 f_0 f_1 (a_s^2 k^2 - 2)\cos(k\zeta_s) e^{-a_s^2 k^2/4}$$

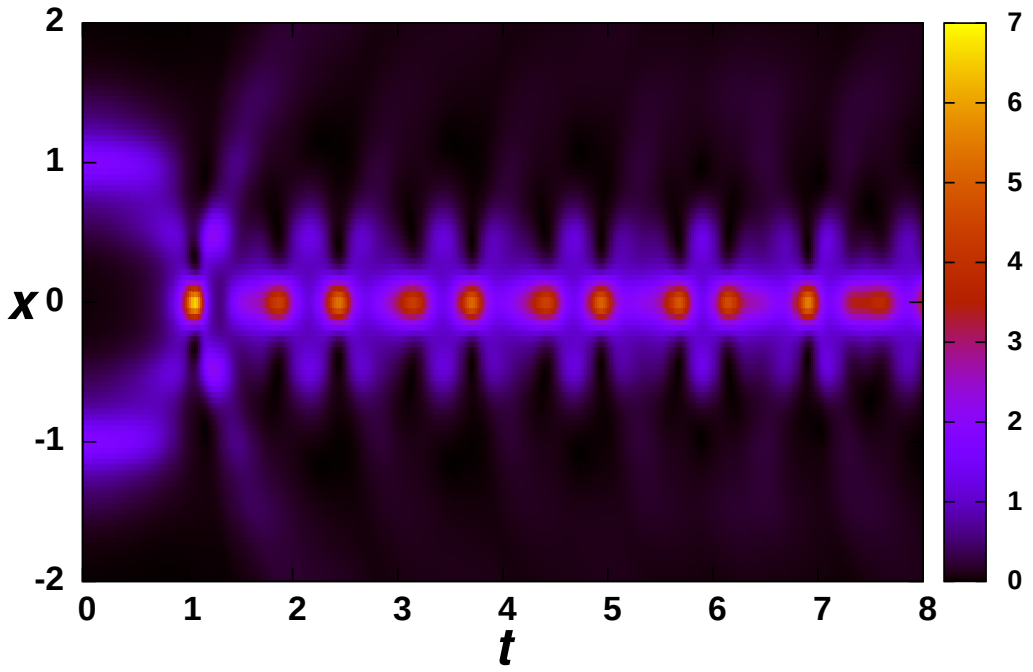

Figure 8. (Color on-line) The density plot corresponding to the results shown in Fig. 7.

$$+ 2\beta k^2 f_1^2 (2a_s^2 k^2 - 1)\cos(2k\zeta_s) e^{-a_s^2 k^2} + \frac{2gN}{\sqrt{2\pi} a_s^3} \tag{44}$$
$$- \frac{6NF}{\pi a^4} + \frac{4N}{\pi a^3}\frac{\partial F}{\partial a}\bigg|_{a=a_s} - \frac{N}{\pi a^2}\frac{\partial^2 F}{\partial a^2}\bigg|_{a=a_s},$$

$$\omega_\zeta^2 = -\frac{\partial \zeta_{tt}}{\partial \zeta} = 2\alpha - 2\beta f_1 k^2 \left[f_0 e^{-a_s^2 k^2/4}\cos(k\zeta_s) + f_1 e^{-a_s^2 k^2}\cos(2k\zeta_s)\right] \tag{45}$$
$$- \frac{N}{2\pi a^2}\frac{\partial^2 F}{\partial \zeta^2}\bigg|_s .$$

Finally, in Fig. 9 we show results for both frequencies of small oscillations of the solitons, ω_a and ω_ζ, comparing the VA predictions to numerical findings. In the left panel we consider perturbations of their widths, where we observe a good agreement of the numerical results with the VA. The parameters in this case are $\beta = 0$, $\Lambda = 0.5$, $f_0 = 1$, and $f_1 = 0.5$. In the right panel of this figure, we follow the same procedure by comparing the numerical results with VA for frequencies related to small oscillations of the center-of-mass, near $\zeta = 0$. Note that the numerical results displayed in the left panel of Fig. 9 show that the frequency of the width oscillations grows almost linearly with N, in both cases of $\beta = 0$ and $\beta = 6$. The VA gives a good description of the results for smaller values of N, and the approximation is improved for larger values of β. In the case of the center-of-mass oscillations, displayed only for $\beta = 0$, we also observe that the frequency increases with N, although in this case the VA is less accurate, especially

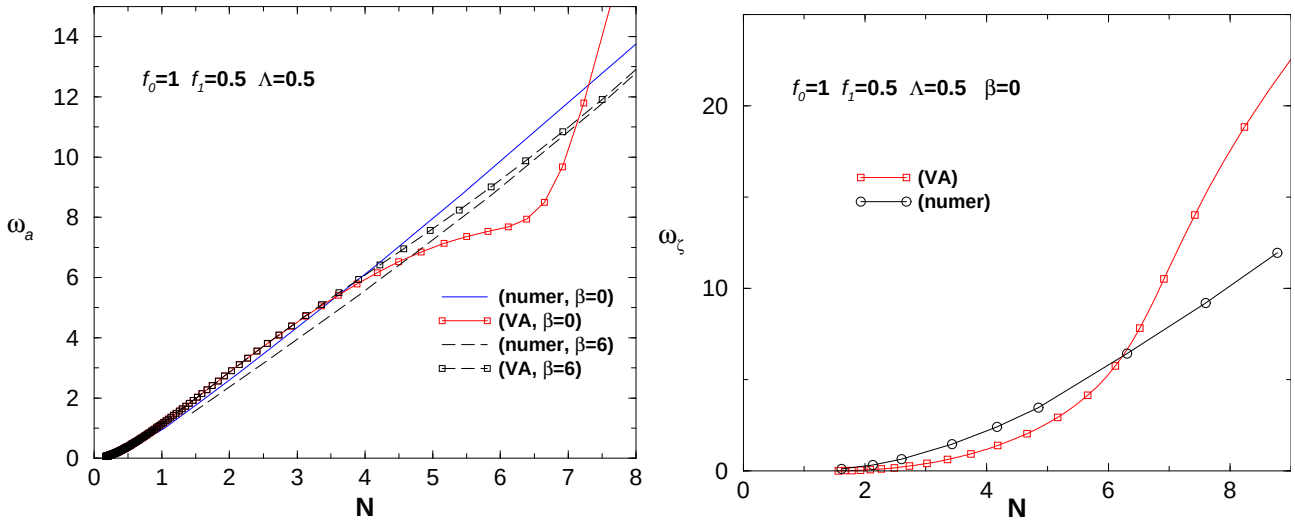

Figure 9. The left panel: variational results (44) (red-solid lines with squares) and numerical solutions (black-solid lines with circles) for frequencies of small oscillations of perturbed solitons, ω_a, as functions of N. The parameters, as given in the panel, are $f_0 = 1$, $f_1 = 0.5$, $\Lambda = 0.5$, and $\beta = 0$. The right panel: for the same parameters, we show the corresponding variational results for the frequencies of oscillations of the soliton's center of mass, ω_ζ [as given by Eq. (45)], compared to the numerical calculations.

for larger N, which is explained by the inadequate shape of the underlying ansatz (36).

5. Conclusion

The objective of this work is to expand the range of settings based on dipolar BECs, by introducing a model in which atoms or molecules in the free condensate carry no dipolar moments, but local moments are induced by a spatially modulated external polarizing field. The DDI (dipole-dipole interactions) in this setting give rise to an effective nonlocal nonlinear lattice in the condensate. In the case when the respective interactions are attractive, they support bright solitons. We have investigated conditions for the existence of such solitons (including the situation when the attractive DDI competes with the local repulsion) in the semi-analytical form, by dint of the VA (variational approximation) based on the Gaussian ansatz. The results were verified by comparison with numerical solutions of the respective one-dimensional GPE (Gross-Pitaevskii equation). The stability of the soliton families exactly obeys by the VK criterion. The dynamics of solitons and interactions between them, including merger into breathers, were investigated too. In particular, it was found that the dynamical version of the VA provides for a good prediction for frequencies of small oscillations of perturbed solitons.

An issue of obvious interest is to extend the analysis reported here for 2D configurations.

Acknowledgments

This work was partially supported by the Brazilian agencies Fundação de Amparo à Pesquisa do Estado de São Paulo (FAPESP), Conselho Nacional de Desenvolvimento Científico e Tecnológico (CNPq) and Coordenação de Aperfeiçoamento de Pessoal de Nível Superior (CAPES). BAM was supported, in a part, by the grant from the German-Israeli Foundation No. I-1024-2.7/2009.

References

[1] Griesmaier A, Werner J, Hensler S, Stuhler J and Pfau T 2005 *Phys. Rev. Lett.* **94** 160401; Beaufils Q, Chicireanu R, Zanon T, Laburthe-Tolra B, Maréchal E, Vernac L, Keller J-C and Gorceix O 2008 *Phys. Rev. A* **77** 061601

[2] Lu M, Burdick N Q, Youn S H and Lev B L 2011 *Phys. Rev. Lett.* **107**, 190401

[3] Aikawa K, Frisch A, Mark M, Baier S, Rietzler A, Grimm R and Ferlaino F 2012 *Phys. Rev. Lett.* **108** 210401

[4] Lewenstein M, Sanpera A and Ahufinger V 2012 *Ultracold Atoms in Optical Lattices: Simulating quantum many-body systems* (Oxford University Press: Oxford, UK).

[5] Baranov M 2008 *Phys. Rep.* **464** 71

[6] Lahaye T, Menotti C, Santos L, Lewenstein M and Pfau T 2009 *Rep. Prog. Phys.* **72** 126401

[7] Carr L D, DeMille D, Krems R V and Ye J 2009 *New J. Phys.* **11** 055049

[8] Saito H, Kawaguchi Y and Ueda M 2009 *Phys. Rev. Lett.* **102** 230403; Klawunn M and Santos L 2009 *Phys. Rev. A* **80** 013611; Nath R and Santos L 2010 *Phys. Rev. A* **81** 033626; Maluckov A, Gligorić G, Hadžievski L, Malomed B A and Pfau T 2012 *Phys. Rev. Lett.* **108** 140402; Łakomy K, Nath R and Santos L 2012 *Phys. Rev. A* **86** 023620; Maluckov A, Gligori ć G, Hadžievski L, Malomed B A and Pfau T 2013 *Phys. Rev. A* **87** 023623; Nikolić B, Balaž A and Pelster A 2013 *Phys. Rev. A* **88** 013624

[9] Lahaye T, Metz J, Fröhlich B, Koch T, Meister M, Griesmaier A, Pfau T, Saito H, Kawaguchi Y and Ueda M 2008 *Phys. Rev. Lett.* **101** 080401; Metz J, Lahaye T, Fröhlich B, Griesmaier A, Pfau T, Saito H, Kawaguchi Y and Ueda M 2009 *New J. Phys.* **11** 055032

[10] Łakomy K, Nath R and Santos L 2012 *Phys. Rev. A* **85** 033618; Li Y, Liu J, Pang W and Malomed B A 2013 *Phys. Rev. A* **87** 013604

[11] Tikhonenkov I, Malomed B A and Vardi A 2008 *Phys. Rev. Lett.* **100** 090406; Köberle P, Zajec D, Wunner G and Malomed B A 2012 *Phys. Rev. A* **85** 023630; Kishor Kumar R, Muruganandam P, and Malomed B A 2013 *J. Phys. B: At. Mol. Opt. Phys.* **46** 175302.

[12] Cuevas J, Malomed B A, Kevrekidis P G and Frantzeskakis D J 2009 *Phys. Rev. A* **79** 053608

[13] Young-S L E, Muruganandam P and Adhikari S K 2011 *J. Phys. B: At. Mol. Opt. Phys.* **44** 101001

[14] Gligorić G, Maluckov A, Hadžievski L and Malomed B A 2009 *J. Phys. B: At. Mol. Opt. Phys.* **42** 145302

[15] Adhikari S K and Muruganandam P 2011 *J. Phys. B: At. Mol. Opt. Phys.* **44** 121001; 2012 *J. Phys. B: At. Mol. Opt. Phys.* **45** 045301

[16] Micheli A, Pupillo G, Buchler H P and Zoller P 2007 *Phys. Rev. A* **76** 043604

[17] Li Y, Liu J, Pang W and Malomed B A 2013 *Phys. Rev. A* **88** 053630

[18] Abdullaev F Kh, Gammal A, da Luz H L F, Salerno M and Tomio L 2012 *J. Phys. B: At. Mol. Opt. Phys.* **45** 115302

[19] Kartashov Y V, Malomed B A and Torner L 2011 *Rev. Mod. Phys.* **83** 247

[20] Abdullaev F Kh, Gammal A, Malomed B A and Tomio L 2013 *Phys. Rev. A* **87** 063621

[21] Ghanbari S, Kieu T D, Sidorov A and Hannaford P 2006 *J. Phys. B: At. Mol. Opt. Phys.* **39** 847; Abdelrahman A, Hannaford P and Alameh K 2009 *Opt. Express* **17** 24358

[22] Potter B G, Tikare V and Tuttle B A 2000 *J. Appl. Phys.* **87** 4415
[23] Yi S and You L 2000 *Phys. Rev. A* **61** 041604; Deb B and You L 2001 *Phys. Rev. A* **64** 022717; McCarthy T J, Timko M T and Herschbach D R 2006 *J. Chem. Phys.* **125** 133501; Li Z D, Li Q Y, He P B, Liang J Q, Liu W M and Fu G S 2010 *Phys. Rev. A* **81** 015602; Golomedov A E, Astrakharchik G E and Lozovik Y E 2011 *Phys. Rev. A* **84** 033615
[24] Sinha S and Santos L 2007 *Phys. Rev. Lett.* **99** 140406
[25] Salasnich L 2002 *Laser Phys.* **12** 198; Salasnich L, Parola A and Reatto L 2002 *Phys. Rev. A* **65** 043614
[26] Bortolotti D C E et al. 2006 *Phys. Rev. Lett.* **97** 160402
[27] Kawaguchi Y, Saito H and Ueda M 2006 *Phys. Rev. Lett.* **96** 080405
[28] Swislowski T et al. 2011 *Phys. Rev. A* **83** 063617
[29] A de Paz et al. 2013 *Phys. Rev. A* **87** 051609
[30] Wall M L, Maeda K and Carr L 2013 Ann. Phys. **525** 845
[31] Ni K-K, Ospelkaus S, Wang D, Quéméner G, Neyenhuis B, de Miranda M G H, Bohn J L, Ye J and Jin D S 2010 *Nature (London)* **464** 29
[32] Yi S and You L 2000 *Phys. Rev. A* **61** 041604
[33] Deb B and You L 2001 *Phys. Rev. A* **64** 022717
[34] McCarthy T J, Timko M T, and Herschbach D R 2006 *J. Chem. Phys.* **125** 133501
[35] Li Z D, Li Q Y, He P B, Liang J Q, Liu W M and Fu G S 2010 *Phys. Rev. A* **81** 015602
[36] Golomedov A E, Astrakharchik G E and Lozovik Y E 2011 *Phys. Rev. A* **84** 033615
[37] te Velde G, Bickelhaupt F M, Baerends E J, Guerra C F, Van Gisbergen S J A, Snijders J G and Ziegler T 2001 *J. Comp. Chem* **22** 931
[38] Brtka M, Gammal A and Tomio L 2006 *Phys. Lett. A* **359** 339
[39] Vakhitov M and Kolokolov A 1973 *Radiophys. Quant. Electron.* **16** 783
[40] Sakaguchi H and Malomed B A 2005 *Phys. Rev. E* **72** 046610
[41] Abdullaev F Kh and Garnier J 2005 *Phys. Rev. A* **72** (2005) 061605(R)
[42] Abdullaev F Kh, Abdumalikov A A and Galimzyanov R M 2007 *Phys. Rev. A* **367** 149
[43] Kartashov Y V, Vysloukh V A and Torner L 2008 *Opt. Lett.* **33** 1774